White Rose Research Online

eprints@whiterose.ac.uk
https://eprints.whiterose.ac.uk
Universities of Leeds, Sheffield and York

Deposited via The University of York.

White Rose Research Online URL for this paper:
https://eprints.whiterose.ac.uk/id/eprint/246085/

Version: Published Version

Article:
(2026) Neoclassical tearing mode seeding by Alfvén eigenmode coupling in MAST-U. Nuclear Fusion. 126007. ISSN: 1741-4326

https://doi.org/10.1088/1741-4326/aea348

Reuse
This article is distributed under the terms of the Creative Commons Attribution (CC BY) licence. This licence allows you to distribute, remix, tweak, and build upon the work, even commercially, as long as you credit the authors for the original work. More information and the full terms of the licence here:
https://creativecommons.org/licenses/

Takedown
If you consider content in White Rose Research Online to be in breach of UK law, please notify us by emailing eprints@whiterose.ac.uk including the URL of the record and the reason for the withdrawal request.

UNIVERSITY OF LEEDS
University of Sheffield
UNIVERSITY of York

nuclear fusion
IAEA

PAPER • **OPEN ACCESS**

Neoclassical tearing mode seeding by Alfvén eigenmode coupling in MAST-U

To cite this article: Kitt Thomas *et al* 2026 *Nucl. Fusion* **66** 126007

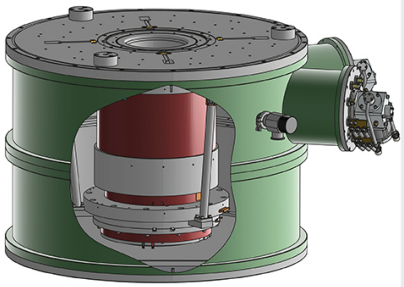
View the article online for updates and enhancements.

You may also like

- Excitation of the beta-induced Alfvén eigenmodes by a magnetic island
V.S. Marchenko and S.N. Reznik
- Experimental observation of beta-induced Alfvén eigenmodes during strong tearing modes on the EAST tokamak in fast-electron plasmas
M Xu, W Chen, L Q Hu et al.
- Excitation of the beta-induced Alfvén eigenmode by a plasma flow around the magnetic island
V.S. Marchenko, A. Panwar, S.N. Reznik et al.

Unit 6 Acton Park, The Vale,
London W3 7QE, United Kingdom
CRYOGENIC
Tel: +44 20 8743 6049
Email: sales@cryogenic.co.uk
www.cryogenic.co.uk

10.5 Tesla
CRYOGEN-FREE GYROTRON MAGNET SYSTEM FOR FUSION



10.5 Tesla
Cavity Field Strength

Ø 240 mm
Room Temperature Bore (Ø 290 mm at the emitter)

±0.5 mm
Electron Beam Shift via Dipole Coils

- With Integrated X–Y Dipole Steering Coils
- Field Homogeneity: ±0.1% in the cavity region
- Magnetic Axis Displacement: <0.30 mm
- Gyrotron Mass: Supports up to 2,000 kg
- Automation: Full PLC/LabVIEW Remote Control Interface



System pictured with the Karlsruhe Institute of Technology (KIT) team

This content was downloaded from IP address 144.32.240.146 on 29/09/2026 at 11:00

OPEN ACCESS
IOP Publishing | International Atomic Energy Agency
Nuclear Fusion
Nucl. Fusion **66** (2026) 126007 (7pp)
https://doi.org/10.1088/1741-4326/aea348

Neoclassical tearing mode seeding by Alfvén eigenmode coupling in MAST-U

Kitt Thomas[1,*], Laszlo Bardoczi[2], Kieran Gibson[1], Juan Ruiz Ruiz[1], Mykola Dreval[3], David Ryan[4], Ken McClements[4], Clive Michael[5] and MAST-U team[4,a]

[1] York Plasma Institute, University of York, York, United Kingdom of Great Britain and Northern Ireland
[2] University of California Irvine, CA, United States of America
[3] Kharkov Institute of Physics and Technology, Kharkov, Ukraine
[4] UKAEA, Culham Campus, Abingdon, United Kingdom of Great Britain and Northern Ireland
[5] University of California Los Angeles, CA, United States of America

E-mail: kitt.thomas@york.ac.uk

Received 21 June 2026, revised 3 August 2026
Accepted for publication 7 September 2026
Published 18 September 2026

Abstract

We present evidence of tearing mode seeding by nonlinear three-wave coupling of Alfvén eigenmodes in a tokamak plasma. Here, a $m,n = 2,1$ magnetic island appears to be seeded in a MAST-U discharge by coupling of $n = 2$ and $n = 3$ Alfvén eigenmodes, which is demonstrated by increased squared normalised bicoherence calculated from magnetic probes preceding tearing mode onset. This observation offers a new explanation for tearing modes that would be otherwise addressed as spontaneous, and indicates three-wave coupling can seed 2,1 magnetic islands in plasmas without pre-existing $n \geqslant 2$ tearing modes. Further, this mechanism has the potential to be more prevalent in burning plasmas expected in future fusion devices.

Keywords: tearing modes, Alfvén eigenmodes, nonlinear coupling, bicoherence

(Some figures may appear in colour only in the online journal)

1. Introduction

The neoclassical tearing mode (NTM) is a performance-limiting magnetohydrodynamic (MHD) instability common in high-β tokamak fusion plasmas [1]. NTMs are observed as chains of 'magnetic islands' in the plasma poloidal cross section, with geometry characterised by poloidal (m) and toroidal (n) mode numbers. These islands facilitate radial transport of particles across their width, degrading confinement and flattening the local radial pressure profile. This flattening then perturbs the local bootstrap current, driving the growth of the island until either it reaches a saturated width or it triggers a disruption [2].

NTM growth is described by the modified Rutherford equation (MRE) [1]. A key implication of the MRE is the existence of a critical island width w_c, above which a magnetic island is unstable and grows until saturation. Producing an unstable NTM therefore requires a MHD trigger mechanism (e.g. sawtooth crash) to 'seed' an island of width $w > w_c$, although in some cases 'spontaneous' NTMs have been observed without a clear trigger mechanism [3]. In these cases it is postulated that a trigger mechanism does exist but is not clearly visible [4] (e.g. seeding by turbulence [5]), or that an initially classically unstable tearing mode grows into an NTM [6].

Another MHD instability of concern in tokamaks is the Alfvén eigenmode (AE). AEs are often driven unstable by energetic particles such as fast ions generated by fusion reactions or neutral beam injection [7], and are resonantly excited at frequencies outside the Alfvén continuum, such as inside 'frequency gaps' for toroidal AEs (TAEs) [8]. These instabilities reduce the confinement of fast ions, degrading

[a] See author list J.R. Harrison *et al* 2026 (https://doi.org/10.1088/1741-4326/ae63e1) MAST-U team.
[*] Author to whom any correspondence should be addressed.

Original content from this work may be used under the terms of the Creative Commons Attribution 4.0 licence. Any further distribution of this work must maintain attribution to the author(s) and the title of the work, journal citation and DOI.

 © 2026 The Author(s). Published by IOP Publishing Ltd on behalf of the IAEA

fusion performance, with the flux of lost particles potentially also damaging the vessel wall [9]. AEs are also observed in other non-uniform plasmas such as the Earth's magnetosphere, where they contribute to thermalising the ion distribution [10].

Previously [11–13], the seeding of $m,n = 2,1$ NTMs by nonlinear three-wave coupling of $n > 1$ tearing modes with 1,1 sawtooth precursors has been observed in DIII-D ITER baseline scenario (IBS) plasmas [14]. Although this mechanism is likely the dominant trigger for 2,1 NTMs in IBS discharges, on account of at least 70% of these plasmas satisfying the necessary frequency matching condition at onset time [15], until now there has been no experimental evidence of this trigger mechanism in other plasmas without pre-existing $n > 1$ tearing modes. Nonlinear coupling between AEs has been observed [16], and indeed coupling of AEs to tearing modes (post-onset) [17, 18], but such coupling involving AEs has not been suggested as a seeding mechanism in any case. We now present evidence of NTM seeding by three-wave coupling of AEs in MAST-U H-mode plasmas, obtained through bicoherence and mode number analysis of Mirnov coil voltage signals. This mechanism offers an explanation for some apparently spontaneous NTMs observed in MAST-U and other tokamaks, while potentially being a significant NTM trigger in future fusion devices with burning plasmas where AEs are expected to be ubiquitous [19]. Furthermore, this mechanism could also affect the forecasting of space weather, where AEs are present [20] and magnetic reconnection is considered a significant mechanism for the transfer of kinetic energy into the Earth's magnetosphere [21].

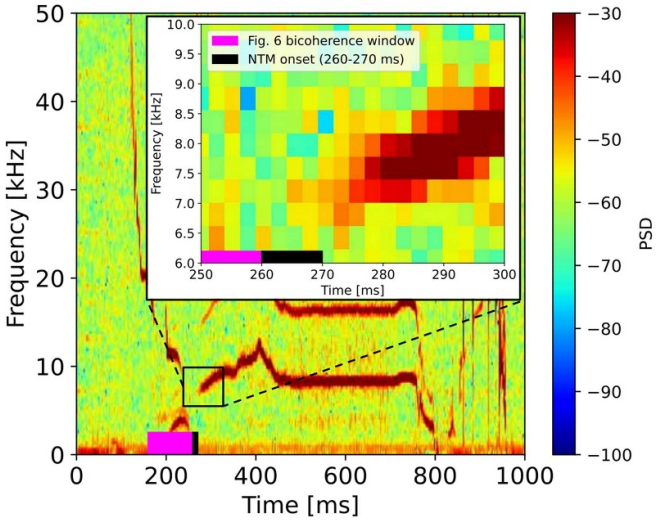


Figure 1. Low frequency Mirnov coil spectrogram showing the onset of the 2,1 NTM at 6–8 kHz at 260–270 ms. A previous NTM exists from 200 to 250 ms at < 5 kHz, but this is not the subject of this study. The Mirnov coil used for this spectrogram is located 21 cm above the midplane at $\phi = 337°$.

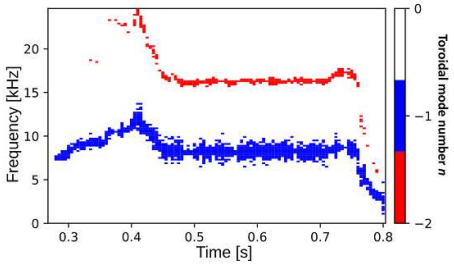


Figure 2. Toroidal mode number analysis of NTM from 260 to 800 ms.

2. Method and results

2.1. Experimental setup

Our observations were conducted in MAST-U discharge #49131, an $I_p = 600$ kA double-null divertor plasma scenario with the following parameters at time of NTM onset: magnetic axis major radius $R_0 = 0.98$ m, minor radius $a = 0.5$ m, toroidal magnetic field $B_T = 0.5$ T, neutral beam heating power $P_{\mathrm{NBI}} = 3.3$ MW, and normalised plasma beta $\beta_{\mathrm{N}} = \beta a B_T / I_{\mathrm{p}} \approx 2.3$, where β is the ratio of plasma pressure to magnetic pressure. The core electron number density is $n_{\mathrm{e}} = 3 \times 10^{19}$ m^{-3} and core electron temperature is $T_{\mathrm{e}} = 1.1$ keV.

Information concerning the structure of MHD modes such as magnetic islands is inferred using outboard Mirnov coil voltage signals, located at either 21 cm above or below the midplane, which detect the vertical magnetic perturbations $\tilde{B}_z$ associated with mode rotation and growth. Modes detected in these signals rotate with frequency $f_{m,n}/n$, with $f_{m,n}$ visible as a continuous trace of high power spectral density in this signal's spectrogram. Mode numbers, amplitudes and rotation frequencies of MHD modes are obtained from Mirnov coil data. For simplicity, the signs of toroidal mode numbers are ignored in the text as they are all negative, which implies the modes all rotate in the co-current direction.

2.2. NTM onset and coinciding modes

From a spectrogram of a single low frequency Mirnov coil signal (see figure 1), we determine onset of the NTM of interest from the earliest visible appearance of the mode from 260–270 ms at frequency $6 - 8$ kHz. The toroidal mode number $n = 1$ is inferred by analysing the variation of the mode's phase with toroidal angle (see figure 2), and the poloidal mode number $m = 2$ is deduced by matching the mode trace in the spectrogram to the charge exchange recombination spectroscopy (CXRS) [22] rotation time trace at the $q = 2$ surface, where $q(r) = m/n$ is the safety factor.

The onset of the $m,n = 2,1$ tearing mode coincides with mode activity from 50–150 kHz, as seen in figure 3, including $n = 2$ and $n = 3$ modes at ~ 130 kHz (toroidal mode numbers obtained in section 2.3). The possible identities of these modes are discussed later in section 2.6

To rule out edge localised modes (ELMs) as a potential NTM seeding mechanism we inspect the D_α signal (figure 4), in which no ELMs are observed within 29 ms of the NTM onset time. Additionally, we may also discard sawtooth crash seeding from the minimum safety factor $q_{\mathrm{min}} \sim 1.6$ at onset time, since $q_{\mathrm{min}} \leqslant 1$ is required for a sawtooth precursor mode

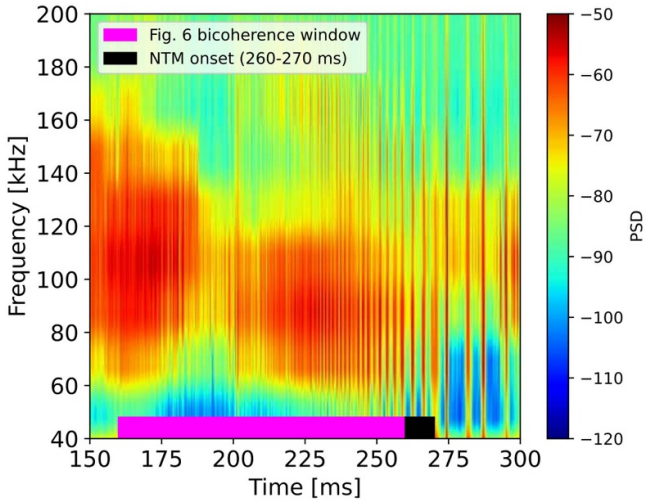


Figure 3. High frequency Mirnov coil spectrogram showing AE activity coinciding with NTM onset. The Mirnov coil used here is located 21 cm above the midplane at $\phi = 355°$.

to be present in the plasma. Fishbone modes are also not visible, also ruling these out as a seeding mechanism. Finally, there is no drop in neutron rate preceding or during NTM onset to suggest any significant fast ion transport associated with (for example) an Alfvénic avalanche [23], hence fast ion redistribution is unlikely to trigger the NTM.

To determine whether the mode is classically seeded, we calculate classical tearing stability at the $q = 2$ surface with `RDCON` [24]. This produces a raw, unnormalised and dimensionless output $\Delta'_{q=2}$ proportional to Δ' in the MRE, meaning a positive value indicates the mode is classically unstable. In figure 5 we see that although $\Delta'_{q=2}$ is positive from 200 to 210 ms, possibly triggering the previous NTM visible at < 5 kHz from 200–250 ms, $\Delta'_{q=2}$ is negative immediately preceding and during onset of the NTM at 260–270 ms. This suggests the plasma is classically stable to tearing modes at the $q = 2$ surface at onset time, ruling out classical seeding for the NTM of interest. The NTM may therefore be classified as spontaneous, meaning nonlinear three-wave coupling remains a plausible trigger in the absence of other seeding mechanisms.

2.3. Bicoherence analysis

The 'squared normalised bispectrum' $b^2(f_1,f_2)$, also referred to as 'bicoherence', is a statistical measure useful for inferring nonlinear wave interactions in a signal such as three-wave coupling. It quantifies the fraction of wave power at frequency (f_1+f_2) generated by quadratic coupling of waves at frequencies f_1,f_2 . The bicoherence takes values from 0 to 1, with a value of 1 implying the wave power at frequency (f_1+f_2) is entirely produced by nonlinear coupling of frequencies f_1,f_2, and 0 implying the wave power at this frequency is entirely spontaneous and/or generated by linear coupling [25]. A high bicoherence value also implies a constant phase relation between the three frequencies $f_1,f_2,(f_3 = f_1+f_2)$, i.e. the

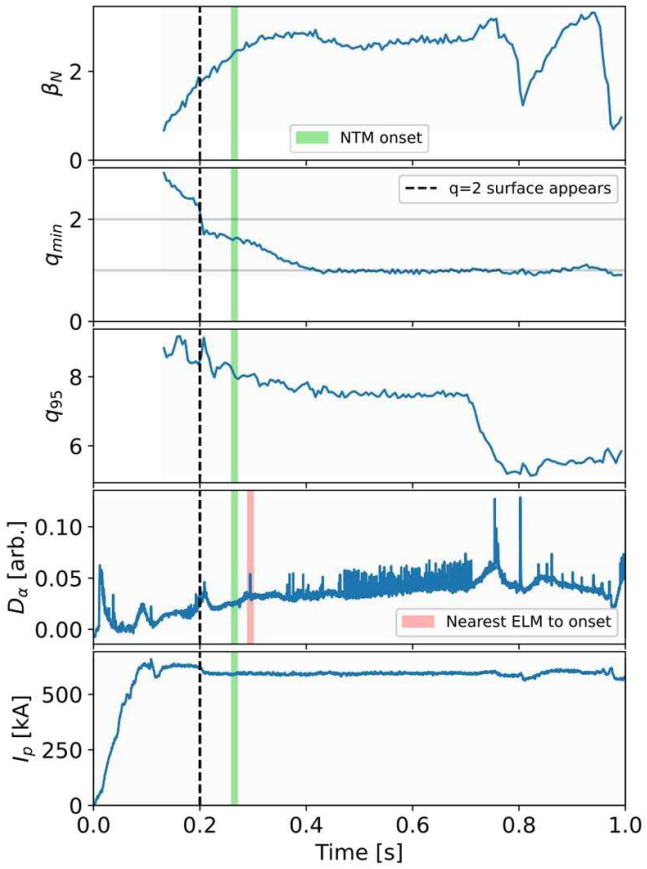


Figure 4. $\beta_N, q_{\mathtt{min}}, q_{95}$ (obtained from MSE-constrained EFIT), D_α and I_p signals over the duration of shot #49131.

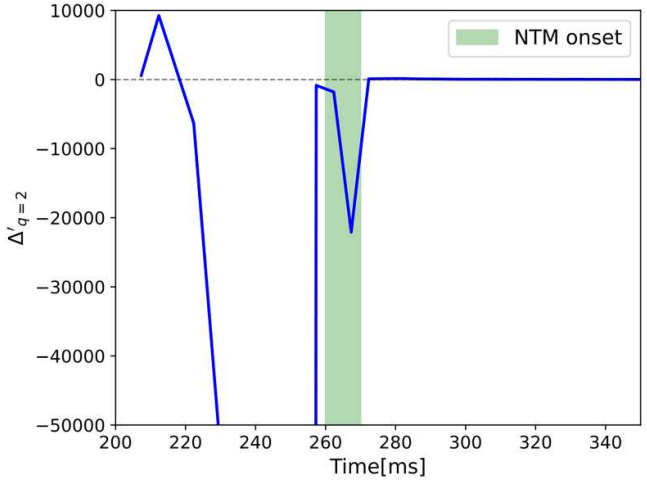


Figure 5. Classical tearing stability Δ' at the $q = 2$ surface around NTM onset. Δ' reaches a minimum of -4.7×10^7 at 247 ms (this point is cropped out of this figure to improve clarity of the trace pre-NTM onset).

sum $\phi_1 + \phi_2 - \phi_3$ is approximately constant across the analysed segments of the time series [26]. Bicoherence may be calculated from Mirnov signal time slices using equation (1):

$$b^2(f_1,f_2) = \left\langle \frac{|\langle F_{i,n}(f_1)F_{i,n}(f_2)F^*_{i,n}(f_1+f_2)\rangle_n|^2}{\langle|F_{i,n}(f_1)F_{i,n}(f_2)|^2\rangle_n \langle|F^*_{i,n}(f_1+f_2)|^2\rangle_n} \right\rangle_i . \quad (1)$$

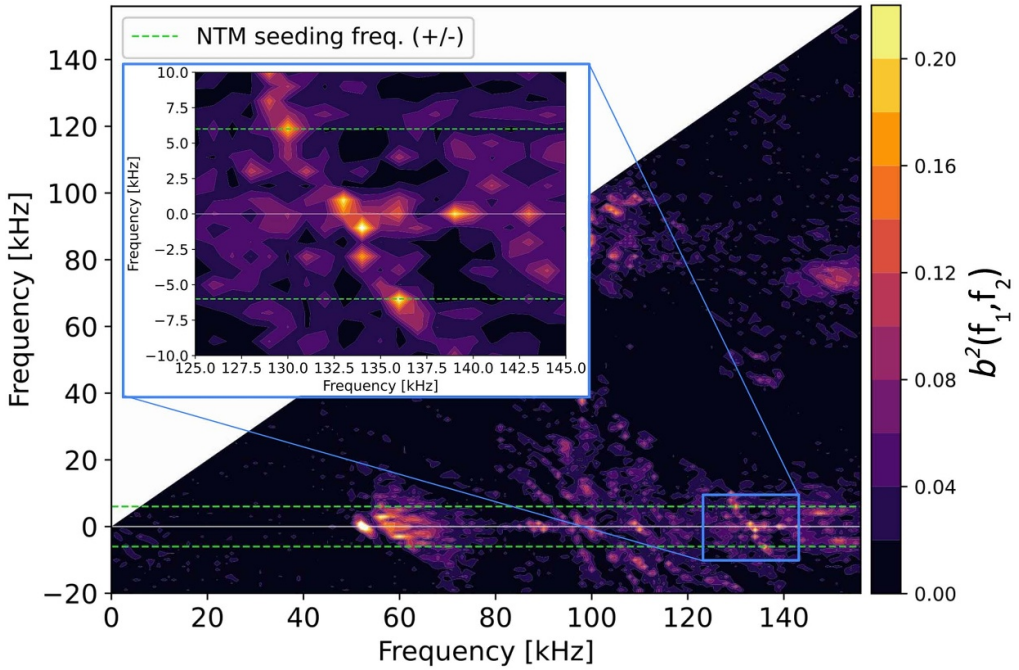


Figure 6. Squared normalised bicoherence b^2 of Mirnov signal calculated with $N = 100$ for the analysis window 160–260 ms.

Here, $\langle \ldots \rangle_n$ and $\langle \ldots \rangle_i$ indicate averaging over n time segments and i Mirnov signals, and $F_{i,n}$ is the Fourier transform of segment n of Mirnov signal i, with $F^*_{i,n}$ its complex conjugate.

In our analysis, we calculate bicoherence over $\Delta t = 100$ ms windows with $N = 100$ segments, yielding a frequency resolution of $f_{\mathtt{res}} = N/\Delta t = 1$ kHz for our bispectra. Each of our 100 ms analysis windows contains 62 500 points, with exactly 625 points in each segment; the high-frequency Mirnov coils (sampling frequency $f_{\mathrm{s}} = 10$ MHz) are downsampled to 625 kHz as we are only interested in the frequency range where AEs are visible ($\lesssim 200$ kHz). Our signals therefore have an effective Nyquist frequency of $f_{\mathrm{N}} = 312.5$ kHz. Finally, we average the bicoherence over 5 high-frequency Mirnov coils to reduce noise.

Before bicoherence is calculated for a signal, the mean is calculated for each of the N segments and subtracted from the corresponding segment. This ensures the signal is stationary before analysis to reduce the presence of artefacts in the bispectrum. We first calculate the bispectrum for the time window 160–260 ms (figure 6), comprising the 100 ms leading up to NTM onset time. This means any bicoherence found in this window should not be the result of the NTM coupling to other modes post-seeding. Error in bicoherence is calculated as the standard error in the mean of the bicoherences calculated over the 5 separate Mirnov coils.

In figure 6 we see strong bicoherence between the NTM seeding frequency 6 kHz and the frequencies 60 kHz, 130 kHz and 150 kHz. The 60 kHz pairing likely corresponds to the coupling of the $n = 0, 1$ modes seen at 60–90 kHz in figure 8, but this cannot be responsible for seeding the NTM at 260–270 ms as the $n = 0$ mode vanishes at 220 ms, so this coupling is ignored. Likewise, the 150 kHz coupling is also ignored but for a different reason, specifically that this bicoherence is unstable in time and its growth does not correlate at all with NTM onset. This leaves just the 130 kHz coupling for our consideration. The (6 kHz, 130 kHz) coupling has a peak bicoherence of $b^2 = (0.20 \pm 0.03)$, and judging from figure 8, may correspond to the quadratic coupling $n = 2, 3$ modes at 120–180 kHz that are present during NTM onset. We investigate this nonlinear coupling further to determine whether this could be responsible for NTM onset.

In figure 7 bicoherence values calculated at ($f_1 = 6$ kHz; $f_2 = 130$ kHz) are plotted against the end times of the 100 ms analysis windows. This means that any bicoherence should be unaffected by any events occurring after the time at which the data is plotted. From the mean of the bicoherence values from 200 to 250 ms we can establish a bicoherence 'noise level' of $b^2_{\mathtt{noise}} \approx 0.04$ (for $\Delta t = 100$ ms and $N = 100$). We then see a significant increase above this baseline for 100 ms analysis windows that end in the time range 256–262 ms, implying strong coupling between the frequencies 6 kHz and 130 kHz that occurs within 5 ms of the 2,1 NTM first appearing on the spectrogram. The coincidence between NTM onset and increase in bicoherence suggests nonlinear three-wave coupling could indeed be responsible for NTM seeding.

We calculate that the NTM reaches a peak nonlinear growth rate of $\frac{1}{w}\frac{\mathrm{d}w}{\mathrm{d}t} = 70\ \mathrm{s}^{-1}$ at 270 ms. Approximating the early NTM growth as linear, we may perform a linear fit to the $n = 1$ amplitude data to estimate the time the NTM begins to grow from zero width. This fitting is performed on the time range 270–300 ms, after the NTM amplitude signal is clear above the noise level in figure 7. This simple modelling predicts the NTM growth begins at ~ 256 ms, coinciding with the start time of the spike in bicoherence. The island growing below the noise level from zero width could therefore explain why

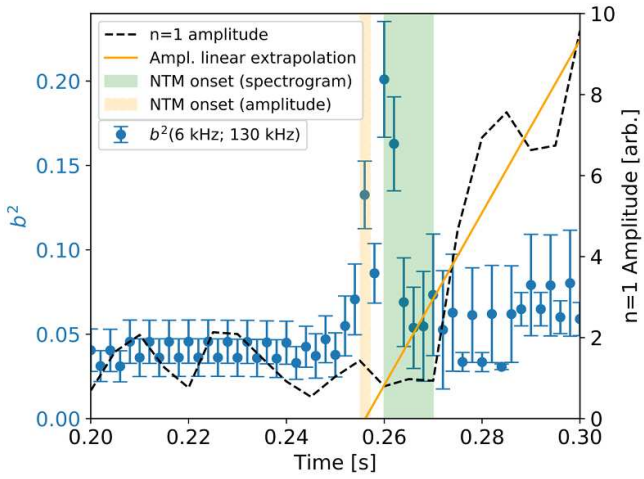


Figure 7. Time traces of $n = 1$ mode amplitude and bicoherence calculated at ($f_1 = 6$ kHz; $f_2 = 130$ kHz) over 100 ms windows with $N = 100$ segments. Note that for bicoherence, the plotted times correspond to the end times of the analysis windows.

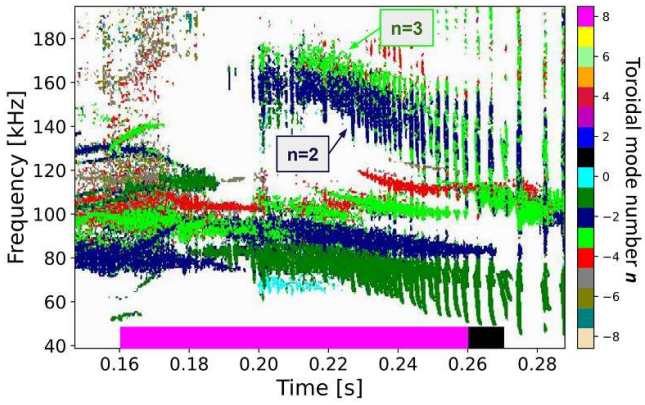


Figure 8. Toroidal mode numbers of AEs coinciding with NTM onset. The colour bars at the bottom of the figure indicate the bicoherence analysis window for figure 6(magenta), and the NTM onset time (black).

the NTM appears in the spectrogram ~ 5 ms after the bicoherence reaches its peak value.

2.4. Convergence analysis

To assess whether the bicoherence observed at ($f_1 = 6$ kHz; $f_2 = 130$ kHz) is spurious or corresponds to legitimate nonlinear coupling, we perform a convergence analysis [27]. We focus on this frequency pair as its bicoherence correlates well with NTM onset and one frequency is close to the NTM onset frequency. When calculating b^2 a high number of segments N is desired to improve statistical convergence, however if N is too large $f_{\mathtt{res}}$ is compromised, and so the poorest tolerable $f_{\mathtt{res}}$ sets the maximum N. Still, a value of bicoherence at $N = \infty$ can be inferred by plotting $1/N$ against b^2, calculating a linear fit of this plot (possible if b^2 varies linearly with $1/N$), then extrapolating the value of b^2 at $1/N = 0$. If b^2 is positive at $1/N = 0$, we may deduce the bicoherence to be distinct from

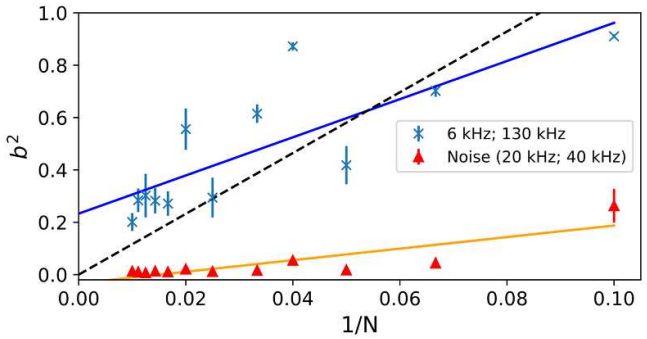


Figure 9. Convergence analysis used to assess the significance of bicoherence measurements calculated for the AE/NTM frequency pair ($f_1 = 6$ kHz; $f_2 = 130$ kHz) and noise reference ($f_1 = 20$ kHz; $f_2 = 40$ kHz) in the 160–260 ms analysis window. The coloured lines show the linear fits used to extrapolate $b^2(N = \infty)$, and the black dotted line is a fit to the ($f_1 = 6$ kHz; $f_2 = 130$ kHz) data forced through the origin for comparison.

background noise. As seen in figure 9, b^2 indeed scales linearly with $1/N$ and converges to $b^2(N = \infty) = (0.23 \pm 0.07)$ for $f_1 = 6$ kHz; $f_2 = 130$ kHz. The noise reference on the other hand, selected as a point on the bicoherence plots far from any visible activity ($f_1 = 20$ kHz; $f_2 = 40$ kHz), is distinct from the b^2 measurements at (6 kHz, 130 kHz) for the full range of N, and converges to a value consistent with zero (-0.03 ± 0.02). These results suggest the bicoherence observed at (6 kHz, 130 kHz) to be distinct from the background noise. In our analysis we considered N =20–100 segments, corresponding to frequency resolutions from $f_{\mathtt{res}} = 200$–1000 Hz.

2.5. AE mode numbers and radial location

The bicoherence considered in figures 6 and 7 implies the coupling of modes in the frequency range 124–136 (130 ± 6) kHz, and the presence of a corresponding bicoherence peak at (136 kHz, -6 kHz) in figure 6 confirms the two high frequencies involved in the three-wave coupling to be 130 and 136 kHz. These frequencies coincide with overlapping $n = 2,3$ AEs. For three-wave coupling between these modes to seed a 2,1 NTM the toroidal mode number matching condition $n_1 \pm n_2 = n_3$ should be satisfied [26], and given that the NTM has $n = 1$ (with a much weaker $n = 2$ harmonic), this could occur through the following interaction:

$$(n_{\mathtt{AE(a)}} = 3) - (n_{\mathtt{AE(b)}} = 2) \rightarrow (n_{\mathtt{NTM}} = 1)\,. \tag{2}$$

The frequency matching condition [25] is then satisfied through the relation:

$$\left(f_{\mathtt{AE(a)}} = 136\mathrm{kHz}\right) - \left(f_{\mathtt{AE(b)}} = 130\mathrm{kHz}\right) \rightarrow \left(f_{\mathtt{NTM}} = 6\mathrm{kHz}\right). \tag{3}$$

From figure 8 we see the $n = 2,3$ AEs first appear in the spectrogram from 190 to 200 ms for the $n = 2$ mode and $\sim$ 200 ms for $n = 3$. At these times, $q_{\mathrm{min}} \gtrsim 2$, hence both modes must be located on a rational surface with $q \gtrsim 2$. This radially constrains the AE locations at NTM onset to the $q = 2$ surface

or beyond i.e. $\rho_{\mathrm{pol}} \gtrsim 0.65$, where $\rho_{\mathrm{pol}} = \sqrt{\psi_{\mathrm{N,pol}}}$ and $\psi_{\mathrm{N,pol}}$ is the normalised poloidal flux.

Furthermore, from the minimum $q = m/n$ we may also deduce the minimum m for each mode; $m \geqslant 4$ for $n = 2$, and $m \geqslant 6$ for $n = 3$. Hence the AEs could satisfy the poloidal mode number matching condition [14] most simply in the interaction shown in equation (4*a*). In this case, both AEs (i.e. 6,3 and 4,2 modes) would be located on the $q = 2$ surface, guaranteeing their eigenfunctions substantially overlap at $\rho_{\mathrm{pol}} = 0.65$ and enabling their coupling to seed a 2,1 NTM at the same location. Alternatively, the combination in equation (4*b*) would require the modes to be situated on the $q = 7/3$ and 5/2 rational surfaces, located at $\rho_{\mathrm{pol}} = 0.71$ and $\rho_{\mathrm{pol}} = 0.73$ respectively, which could also plausibly overlap at the $q = 2$ surface and enable seeding by three-wave coupling. To more conclusively identify the rational surfaces and poloidal mode numbers of these modes however, we require benchmarking against continuum calculations or validation from other diagnostics such as Doppler backscattering (DBS). While DBS is available on MAST-U, it cannot diagnose the modes on this shot due to an unsuitable density profile.

$$(m_{\mathrm{AE(a)}} = 6) - (m_{\mathrm{AE(b)}} = 4) \rightarrow (m_{\mathrm{NTM}} = 2)\,. \tag{4a}$$

$$(m_{\mathrm{AE(a)}} = 7) - (m_{\mathrm{AE(b)}} = 5) \rightarrow (m_{\mathrm{NTM}} = 2)\,; \tag{4b}$$

2.6. Identities of AEs

From the radial range of these AEs, we may infer their rotation frequencies to be in the range $f_{\mathrm{rot}} < 10$ kHz from the CXRS rotation profile. If these modes are TAEs, then their Alfvén gap frequencies are expected to be $f_{\mathrm{gap}} = f_{\mathrm{obs}} - nf_{\mathrm{rot}}$, where f_{obs} is the observed mode frequency in the spectrogram after Doppler shift. This yields a maximum gap frequency of 100–110 kHz for $n = 2, 3$, which is large compared to MAST-U Alfvén gaps ($\sim$ 40-70 kHz) previously described in the literature [28, 29]. Thus these are unlikely to be TAEs. Additionally, these modes cannot be reversed shear AEs (RSAEs) as the safety factor profile is monotonic at NTM onset [7]. We therefore suggest these modes to be other species of AE such as elliptical AEs (EAEs) or global AE (GAEs). Again, for a more conclusive identification, benchmarking against continuum calculations is required.

3. Summary and discussion

We report evidence that NTM seeding by nonlinear three-wave interaction does not necessarily require pre-existing tearing modes or sawteeth within the plasma, as seen for DIII-D, but can occur also from the coupling of AEs. Such evidence is obtained from the Mirnov coil voltage signals of a high-performance MAST-U discharge, for which significant values of bicoherence are calculated immediately preceding NTM onset in a plasma which otherwise lacks an obvious tearing mode trigger. Nonlinear coupling could occur between $m, n = 6, 3$ and $4, 2$ modes around 130 kHz, which would satisfy the necessary mode number and frequency matching conditions for three-wave coupling. We note however that there is uncertainty over the exact values of m for these modes, and the possibility of three-wave coupling seeding the NTM is contingent on the condition $\Delta m = 2$ being satisfied between them.

Nonlinear AE coupling could seed a $m, n = 2, 1$ NTM by similar means to the three-wave coupling of $n > 1$ tearing modes. Specifically, in a plasma where the MRE for the 2,1 NTM initially has form:

$$\frac{\mathrm{d}w_{2,1}}{\mathrm{d}t} = \Gamma^{(0)}_{2,1}\left(w_{2,1}\right) < 0, \tag{5}$$

i.e. the plasma is classically stable to 2,1 NTMs, the coupling of AEs introduces a perturbation Γ_{coupl}. This perturbation is a function of the amplitudes, radial locations and mode numbers of the coupling modes, and is maximised at high mode amplitudes. If this perturbation is sufficiently large such that $\Gamma^{(0)}_{2,1}(w_{2,1}) + \Gamma_{\mathrm{coupl}} > 0$, the plasma is then unstable and a 2,1 tearing mode grows from zero width [11]. Upon exceeding a critical width, the seed island remains unstable and continues to grow even once the transient perturbation from three-wave coupling vanishes.

This mechanism is significant as AEs are expected to be more prevalent in future burning plasmas, where a large population of energetic α-particles generated by deuterium–tritium fusion will more frequently drive AEs unstable [19]. As a result, AE coupling has the potential to be a more significant trigger mechanism in next generation fusion devices such as ITER, in addition to previously known trigger mechanisms such as ELMs or sawtooth crashes. The onset rate of tearing modes in these future devices could therefore be greater than previously expected, thus requiring a greater fraction of generated power to be recirculated into tearing mode control methods such as electron cyclotron current drive. The existence of this mechanism also further highlights the need for effective AE control in future tokamak designs. Moreover, this mechanism also offers a new explanation for spontaneous tearing modes in plasmas where onset coincides with AEs of similar frequencies and differing toroidal mode numbers. The discharge we have studied has behaviour consistent with many others of the same scenario, so we expect this mechanism to also occur in other plasmas of the same or similar scenarios. To obtain an accurate estimate of the proportion of NTMs seeded by AE coupling in MAST-U or other tokamaks, our analysis should be repeated over a representative sample of shots, however such an analysis is beyond the scope of this work.

Magnetic island seeding by AE coupling also has implications for the forecasting of space weather. Magnetic reconnection facilitates the transfer of energy from the solar-wind into the Earth's magnetosphere [21], and this energy transfer is the root cause of space weather [30]. Understanding magnetic reconnection is therefore vital for enabling accurate space weather prediction. Magnetic islands generated by the coupling of AEs in space could therefore plausibly affect space weather models by modulating the transfer of energy into the magnetosphere.

Acknowledgments

This work is supported by the UK Research and Innovation, Engineering and Physical Sciences Research Council, Centre for Doctoral Training in Fusion Energy Science and Technology, under Award No. EP S022430/1. This work has been (part-) funded by the EPSRC Fusion Grant 2022/27 [Grant Number EP/W006839/1]. To obtain further information on the data and models underlying this paper please contact PublicationsManager@ukaea.uk .

ORCID iDs

Kitt Thomas 0000-0002-9442-5768
Laszlo Bardoczi 0000-0002-8280-2423
Juan Ruiz Ruiz 0000-0003-4258-5273
David Ryan 0000-0002-7735-3598
Ken McClements 0000-0002-5162-509X
Clive Michael 0000-0003-1804-870X

References

[1] Buttery R.J., Günter S., Giruzzi G., Hender T.C., Howell D., Huysmans G., Haye R.J.L., Maraschek M., Reimerdes H. and Sauter O. 2000 Neoclassical tearing modes *Plasma Phys. Control. Fusion* **42** B61
[2] Seo J., Kim S., Jalalvand A., Conlin R., Rothstein A., Abbate J., Erickson K., Wai J., Shousha R. and Kolemen E. 2024 Avoiding fusion plasma tearing instability with deep reinforcement learning *Nature* **626** 746–51
[3] Fredrickson E.D. 2002 Observation of spontaneous neoclassical tearing modes *Phys. Plasmas* **9** 548–59
[4] Yang J., Podesta M., Fredrickson E.D., Liu C., Berkery J.W. and Poli F.M. 2023 The role of fast ions in spontaneous neoclassical tearing mode instabilities in NSTX *Plasma Phys. Control. Fusion* **65** 064004
[5] Muraglia M., Agullo O., Poyé A., Benkadda S., Dubuit N., Garbet X. and Sen A. 2017 Amplification of a turbulence driven seed magnetic island by bootstrap current *Nucl. Fusion* **57** 072010
[6] Reimerdes H., Sauter O., Goodman T. and Pochelon A. 2002 From current-driven to neoclassically driven tearing modes *Phys. Rev. Lett.* **88** 105005
[7] Heidbrink W.W. 2008 Basic physics of Alfvén instabilities driven by energetic particles in toroidally confined plasmas *Phys. Plasmas* **15** 055501
[8] Chen L. and Zonca F. 2016 Physics of Alfvén waves and energetic particles in burning plasmas *Rev. Mod. Phys.* **88** 015008
[9] White R.B., Fredrickson E., Darrow D., Zarnstorff M., Wilson R., Zweben S., Hill K., Chen Y. and Guoyong F. 1995 Toroidal Alfvén eigenmode-induced ripple trapping *Phys. Plasmas* **2** 2871–3
[10] Dai L. and Wang C. 2023 Kinetic Alfven wave (KAW) eigenmode in magnetosphere magnetic reconnection *Rev. Mod. Plasma Phys.* **7** 3
[11] Nave M.F.F., Lazzaro E., Coelho R., Belo P., Borba D., Buttery R.J., Nowak S. and Serra F. (EFDA-JET Contributors) 2003 Triggering of neo-classical tearing modes by mode coupling *Nucl. Fusion* **43** 179
[12] Hegna C.C. 1996 Nonlinear tearing mode interactions and mode locking in reversed-field pinches *Phys. Plasmas* **3** 4646–57
[13] Coelho R.M., Lazzaro E., Nave M.F. and Serra F. 1999 Nonlinear coupling of rotating magnetic island triplets *Phys. Plasmas* **6** 1194–202
[14] Bardoczi L., Logan N.C. and Strait E.J. 2021 Neoclassical tearing mode seeding by nonlinear three-wave interactions in tokamaks *Phys. Rev. Lett.* **127** 055002
[15] Bardoczi L., Richner N.J., Logan N.C., Strait E.J., Holcomb C.T., Zhu J. and Rea C. 2024 The root cause of disruptive NTMs and paths to stable operation in DIII-D ITER baseline scenario plasmas *Nucl. Fusion* **64** 126005
[16] Podesta M., Bell R.E., Crocker N.A., Fredrickson E.D., Gorelenkov N.N., Heidbrink W.W., Kubota S., LeBlanc B.P. and Yuh H. 2011 Non-linear dynamics of toroidicity-induced Alfvén eigenmodes on the National Spherical Torus Experiment *Nucl. Fusion* **51** 063035
[17] Jiang M. *et al* 2022 Coupling among neoclassical tearing modes, edge localized modes and Alfvén eigenmodes in HL-2A high β h-mode plasmas *Nucl. Fusion* **62** 076025
[18] Shi P.W. *et al* 2019 Nonlinear mode coupling induced high frequency axisymmetric mode on the HL-2A tokamak *Nucl. Fusion* **59** 086001
[19] Qiu Z., Chen L., Zonca F. and Chen W. 2018 Nonlinear decay and plasma heating by a toroidal Alfvén eigenmode *Phys. Rev. Lett.* **120** 135001
[20] Duan S.P., Dai L., Wang C., Liang J., Lui A.T.Y., Chen L.J., He Z.H., Zhang Y.C. and Angelopoulos V. 2016 Evidence of kinetic Alfvén eigenmode in the near-earth magnetotail during substorm expansion phase *J. Geophys. Res. Space Phys.* **121** 4316–30
[21] Hajra R. 2021 September 2017 space-weather events: a study on magnetic reconnection and geoeffectiveness *Sol. Phys.* **296** 50
[22] Conway N.J., Carolan P.G., Mccone J., Walsh M.J. and Wisse M. 2006 High-throughput charge exchange recombination spectroscopy system on mast *Rev. Sci. Instrum.* **77** 10F131
[23] White R.B., Duarte V.N., Gorelenkov N.N., Fredrickson E.D. and Podesta M. 2020 Simulation of Alfvénic avalanche onset in NSTX *Phys. Plasmas* **27** 022117
[24] Glasser A.H. 2016 The direct criterion of Newcomb for the ideal MHD stability of an axisymmetric toroidal plasma *Phys. Plasmas* **23** 072505
[25] Kim Y.C. and Powers E.J. 1978 Digital bispectral analysis of self-excited fluctuation spectra *Phys. Fluids* **21** 1452–3
[26] Crocker N.A., Peebles W.A., Kubota S., Fredrickson E.D., Kaye S.M., LeBlanc B.P. and Menard J.E. 2006 Three-wave interactions between fast-ion modes in the National Spherical Torus Experiment *Phys. Rev. Lett.* **97** 045002
[27] Cziegler I., Tynan G.R., Diamond P.H., Hubbard A.E., Hughes J.W., Irby J. and Terry J.L. 2015 Nonlinear transfer in heated L-modes approaching the L–H transition threshold in Alcator C-Mod *Nucl. Fusion* **55** 083007
[28] Dreval M.B., Oliver H.J.C., Sharapov S.E., Rivero-Rodriguez J.F., Fitzgerald M., Michael C., Ochoukov R., Velarde L., Cecconello M. and Ryan D. (the MAST-U Team) 2024 Observation of bi-directional global Alfvén eigenmodes in the MAST-U tokamak *Nucl. Fusion* **65** 016043
[29] Blyth R., Fitzgerald M. and Breizman B.N. 2026 Reduced model describing resonance overlap threshold for fast ion transport by toroidal Alfvén eigenmodes *Nucl. Fusion* **66** 026028
[30] Palmroth M., Koskinen H.E.J., Pulkkinen T.I., Toivanen P.K., Janhunen P., Milan S.E. and Lester M. 2010 Magnetospheric feedback in solar wind energy transfer *J. Geophys. Res. Space Phys.* **115** A00I10